Design and characterization of an in vivo injectable hydrogel with effervescently generated porosity for regenerative medicine applications

Louise Griveau, Marianne Lafont, Héloïse Le Goff, Clémence Drouglazet, Baptiste Robbiani, Aurore Berthier, Dominique Sigaudo-Roussel, Najma Latif, Catherine Le Visage, Vincent Gache, et al.

Design and characterization of an in vivo injectable hydrogel with effervescently generated porosity for regenerative medicine applications

Louise Griveau, Marianne Lafont, Héloïse Le Goff, Clémence Drouglazet, Baptiste Robbiani, Aurore Berthier, Dominique Sigaudo-Roussel, Najma Latif, Catherine Le Visage, Vincent Gache, et al.

Full length article

Design and characterization of an *in vivo* injectable hydrogel with effervescently generated porosity for regenerative medicine applications

Louise Griveau [a], Marianne Lafont [b], Héloïse le Goff [c], Clémence Drouglazet [c], Baptiste Robbiani [c], Aurore Berthier [a], Dominique Sigaudo-Roussel [a], Najma Latif [d], Catherine Le Visage [b], Vincent Gache [e], Romain Debret [a], Pierre Weiss [b], Jérôme Sohier [a, *]

[a] *Laboratory for tissue biology and therapeutic engineering (LBTI), CNRS, Université de Lyon, UMR 5305, 7 Passage du Vercors, Lyon cedex 7 69367, France*
[b] *Université de Nantes, Oniris, CHU Nantes, INSERM, Regenerative Medicine and Skeleton, RMeS, UMR 1229, Nantes F-44000, France*
[c] *Université de Lyon, INSA-Lyon, MATEIS, UMR CNRS 5510-7 avenue Jean Capelle, F-69621, Villeurbanne, France*
[d] *Imperial College London, Heart Science Centre, Harefield Hospital, Harefield, Middlesex UB9 6JH, UK*
[e] *Institut NeuroMyogène (INMG), Muscle Nuclear and Cytoskeleton Architecture (MNCA), CNRS UMR 5310-INSERM U1217-UCBL1-Université de Lyon, 8 avenue Rockefeller, Lyon 69008. France*

ARTICLE INFO

Article history:
Received 30 June 2021
Received in revised form 20 November 2021
Accepted 23 November 2021

Keywords:
Porous and injectable hydrogels
Effervescence
Tissue engineering

ABSTRACT

Injectable hydrogels that polymerize directly *in vivo* hold significant promises in clinical settings to support the repair of damaged or failing tissues. Existing systems that allow cellular and tissue ingrowth after injection are limited because of deficient porosity and lack of oxygen and nutrient diffusion inside the hydrogels. Here is reported for the first time an *in vivo* injectable hydrogel in which the porosity does not pre-exist but is formed concomitantly with its *in situ* injection by a controlled effervescent reaction. The hydrogel tailorable crosslinking, through the reaction of polyethylene glycol with lysine dendrimers, allows the mixing and injection of precursor solutions from a dual-chamber syringe while entrapping effervescently generated CO_2 bubbles to form highly interconnected porous networks. The resulting structures allow preserving modular mechanical properties (from 12.7 ± 0.9 to 29.9 ± 1.7 kPa) while being cytocompatible and conducive to swift cellular attachment, proliferation, in-depth infiltration and extracellular matrix deposition. Most importantly, the subcutaneously injected porous hydrogels are biocompatible, undergo tissue remodeling and support extensive neovascularisation, which is of significant advantage for the clinical repair of damaged tissues. Thus, the porosity and injectability of the described effervescent hydrogels, together with their biocompatibility and versatility of mechanical properties, open broad perspectives for various regenerative medicine or material applications, since effervescence could be combined with a variety of other systems of swift crosslinking.

Statement of significance: A major challenge in hydrogel design is the synthesis of injectable formulations allowing easy handling and dispensing in the site of interest. However, the lack of adequate porosity inside hydrogels prevent cellular entry and, therefore, vascularization and tissue ingrowth, limiting the regenerative potential of a vast majority of injectable hydrogels. We describe here the development of an acellular hydrogel that can be injected directly *in situ* while allowing the simultaneous formation of porosity. Such hydrogel would facilitate handling through injection while providing a porous structure supporting vascularization and tissue ingrowth.

1. Introduction

Hydrogels are promising materials in the biomedical field, owing to their proven biocompatibility, similarity to native extracellular matrix and modularity in terms of stiffness and cell adhesion [1–3]. However, one of the major need for hydrogel applications in clinical settings is to develop injectable systems that can polymerize *in situ* to conform accurately to irregularly shaped cavities and integrate to adjacent tissues via minimally invasive surgery [4–6]. Such hydrogels would cost-effectively shorten the surgical operation time and hospital stay, minimize the damaging effects on tissues, reduce scar size and lower post-operative pain.

EPH, effervescent porous hydrogel; DGL, poly (L-lysine) dendrimers; PEG, polyethylene glycol; Pc, potassium carbonate; Gaa, glacial acetic acid

* Corresponding author.
E-mail address: jerome.sohier@ibcp.fr (J. Sohier).

https://doi.org/10.1016/j.actbio.2021.11.036

Once injected, and to be used as support for regeneration, hydrogels should allow efficient cellular and tissue ingrowth with blood vessel neoangiogenesis to prevent hypoxia [7]. However, hydrogel candidates that can be readily infiltrated and colonized by cells without preformed porosity are so far limited and related to poor mechanical stability and versatility [8–10]. The induction of porosity inside injectable hydrogels is therefore critical for regenerative purposes. A variety of techniques such as electrospinning [11], freeze drying [12,13], gas/salt leaching [14,15], emulsion templating [16,17], phase separation [18] or gas foaming techniques using CO_2 [19–24] have been proposed to induce a porous structure inside hydrogels. However, even though these approaches are interesting, they are not suitable with direct injection due to mandatory production steps beforehand or to the use of harsh solvents. Moreover, if some instances have been able to combine the formation of a porosity with injectability [24], they generally fail to address the challenge of direct *in situ* injectability or to provide adequate porosity for cellular infiltration and tissue ingrowth.

Among gas foaming techniques, the use of effervescent reactions hold promise to generate porosity while preserving injectable potential of hydrogels due to their inert and non-toxic nature, lack of organic solvents [25,26] and preservation of the biochemical integrity of proteins [27,28]. They provide a convenient tool to create porosities in a variety of materials, such as cement to create bone grafts [29,30], PLLA or PEG hydrogels for cartilage regeneration [31,32] or elastin-like recombinamers [33] for connective tissue support. However, in all these instances, slow crystallization or crosslinking speeds impose additional steps to be able to entrap CO_2 bubbles inside the network, which are non-transposable to *in situ* delivery systems [34]. To allow the formation of porosity during an injection, we hypothesized that the effervescence should be concomitant to the hydrogel polymerization.

These conditions are present in our candidate formulations, based on recently developed poly (L-lysine) dendrimers (DGL) and N-hydroxysuccinimide (NHS) bi-functionalized polyethylene glycol (PEG) hydrogels, which present the advantages of a swift and tailorable crosslinking (seconds to minutes), extensively controllable mechanical properties (from 8 to 90 kPa), inherent interactions with cells through polycationic charges brought by the DGL and biocompatibility [35,36]. Thus we hypothesized that the introduction of potassium carbonate (Pc) and glacial acetic acid (Gaa) as CO_2 producers in the DGL/PEG hydrogels' precursors, to allow an effervescent reaction to occur, could be a facile strategy enabling the formation of a porosity inside DGL/PEG hydrogels while preserving their injectable and mechanical versatility potential as illustrated in Fig. 1. To investigate this hypothesis, we designed and characterized injectable and porous hydrogel systems based on effervescence and studied the cytocombatibility and biocompatibility of these formulations for tissue engineering applications.

2. Materials and methods

2.1. Non-porous hydrogel preparation

Poly(L-lysine) dendrimers of third generation (DGL), (molecular weight of 22000 g/mol, Colcom, France) and Poly(ethylene glycol) (PEG)-bis(N-succinimidyl succinate) (PEG-NHS, 2000 g/mol, Sigma Aldrich) were solubilized at 400 mg/mL in phosphate buffered saline (PBS, Euromedex) and DMSO (Sigma Aldrich) respectively before use. Stock solutions of PEG-NHS in DMSO and DGL in PBS (400 mg/mL) were added to the adjusted volume of PBS to obtain the desired concentrations (i.e; 1.6/25, 2/25 and 2/37 mM DGL/PEG) in 2 ml conical tubes (Maxymum Recovery, Axygen) followed by vigorous homogenization. To form cylinders, 400 µL of hydrogel precursors were allowed to crosslink inside the tubes to then be retrieved and sectioned using a vibratome (7550 Integraslice) at a 50 Hz frequency, 1 µm amplitude and a slow blade speed of 0.10 to 0.15 mm/s to obtain hydrogel discs of 2 or 3 mm high and 9.1 mm diameter. To form drops, 90 µL of the hydrogel precursor mix were swiftly deposited onto a PTFE plate, immediately after homogenization. Hydrogels were allowed to crosslink for 10 min in wet chambers, detached from the hydrophobic surface and immediately used for subsequent experiments without any washing.

2.2. Time needed to obtain DGL/PEG self-standing hydrogel

The time needed to obtain self-standing hydrogels made of DGL and PEG-NHS was investigated by adding DGL in PBS in a small glass vial (8 × 25 × 35 mm) under agitation with a magnetic rod (5 mm long). The vial was placed at exactly 4 cm from the magnetic stirrer and the time needed to form the self-standing material was defined as the time needed to halt the magnetic rod after adding the PEG-NHS in DMSO to the mix at room temperature (RT) to obtain a final volume of 50 µL.

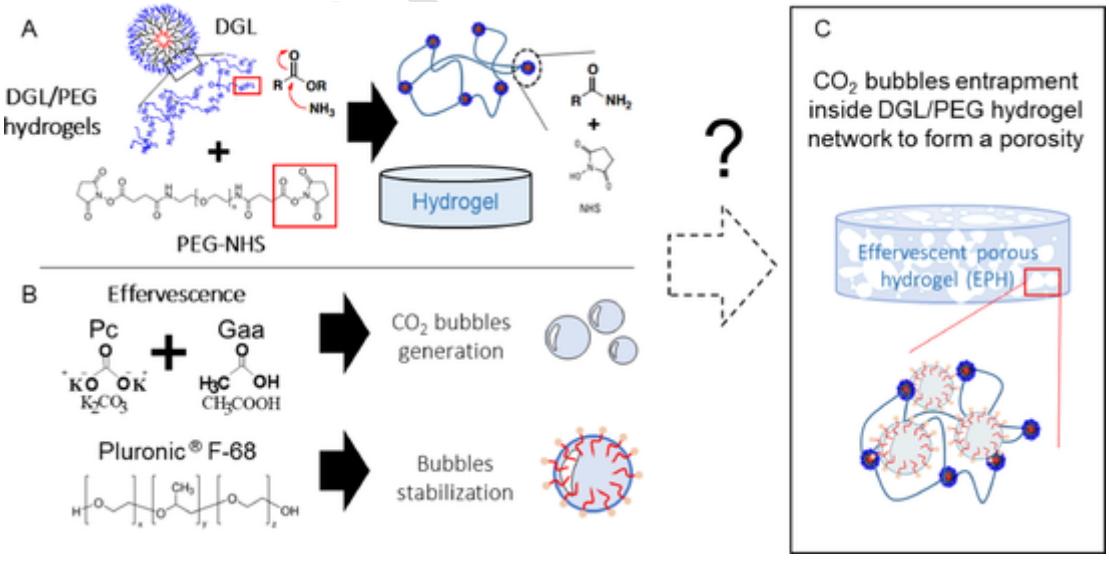

Fig. 1. Schematic representation of the innovative approach developed to realize effervescent porous hydrogels (EPH). DGL and Pc are combined in a compartment of a dual-chamber syringe, PEG, Gaa and a surfactant (the pluronic® F-68) are combined in the second compartment. Once injected through the static mixing nozzle, (A) DGL and PEG react to form the self-standing material while (B) Gaa and Pc reaction generate CO_2 bubbles stabilized by the pluronic® F-68. (C) The appropriate parameters were found to control the entrapment of CO_2 bubbles inside the hydrogel network enabling the creation of the porous structure.

2.3. Interaction of effervescent reactions with DGL/PEG hydrogel precursors

Glacial acetic acid from Carlo Erba was used as received at 17.67M. Potassium carbonate (Sigma Aldrich) was used at saturation in distillated water (8.1 M). Potassium carbonate (Pc) was mixed with glacial acetic acid (Gaa) in phosphate-buffered saline (PBS) to obtain various molar ratios (from 2:1 to 1:1 Acid:Base) and various final molarities (0.5; 1.1 and 1.5 M). The effervescence power and CO_2 bubbles generation were visually assessed. The pH of the solutions after effervescence was monitored at 25˚C using a pH meter (Mettler Toleda, FiveEasy) at various time points. Then, the effect of Gaa:Pc on DGL/PEG hydrogels was studied by adding Gaa:Pc solutions at various ratios (1.33:1 and 1.75:1) and a 1.1 M final molarity (i.e. Gaa at 0.707 M and 0.635 M and Pc at 0.405 M and 0.477 M for 1.75:1 and 1.33:1 molar ratios respectively) to DGL and PEG precursors followed by vigorous homogenization. The effect of a non-ionic surfactant (pluronic® F-68, Thermo fisher scientific) on hydrogel crosslinking was also studied by replacing the buffer with solutions of surfactant in PBS (from 1.7 % up to 7.5 %). Fluorescent non-porous 2/25 mM DGL/PEG hydrogel drops containing various Gaa:Pc molar ratios and pluronic® F-68 concentrations were also prepared using fluorescein-labelled DGL (Colcom) at 0.2 % of the final DGL concentration. After crosslinking, hydrogel drops were transferred into 48 well plates, immersed in PBS (600 μL) without washing or post formulation treatments and incubated at 37 ˚C. After 24 h, supernatants were harvested, and their fluorescence measured using a fluorescence microplate reader (TECAN infinite® 200) at excitation 485 nm and emission 535 nm.

2.4. Porous DGL/PEG hydrogel formulation using an effervescent approach

Effervescent porous DGL/PEG hydrogels (EPH) were prepared by mixing DGL and Pc at desired concentration in PBS in a conical tube (mix 1) to obtain a 200 μL final volume and Pluronic® F-68, Gaa and PEG-NHS in DMSO at desired concentration in a second conical tube (mix 2) at a 200 μL final volume. Both mixes were extensively homogenized and tubes immersed in 37˚C water bath. For manual homogenization of EPH, the mix 2 was added to the mix 1 and homogenized by repeated pipetting. The injectability of EPH was studied by transferring both 200 μL mixes in different compartments of a dual-chamber syringe (adhesive dispensing Ltd) at a ratio 1:1. Both mixes were then injected into a 2.0 mL conical tube through a static mixing nozzle (adhesive dispensing Ltd) to obtain a 400 μL final volume. After crosslinking, EPH were immersed in PBS and their volume expansion was quantified as the ratio between the volume of EPH after reticulation and non-porous hydrogels of the same concentrations and same initial volume of liquid precursors (400 μL). EPH were then removed from tubes and manually cut to obtain 2 or 3 mm-high cylinders. Injected or manually homogenized EPH cylinders were prepared with various Gaa:Pc molar ratios (1.33:1; 1.5:1 and 1.75:1) at a final 1.1 M concentration, pluronic® F-68 concentrations (1.7; 3.3 and 5 %) and DGL/PEG concentrations (1.6/25, 2/25 and 2/37 mM). Representative pictures by optic microscopy were performed on injected EPH cylinders, previously stained with a 0.1 % Coomassie brilliant blue G-250 in methanol/acetic acid/water (20/10/70; v/v/v) solution for one hour, followed by three rinsing in PBS.

2.5. Injectability assessment

Injectability was assessed with porous 2/25 and 2/37 mM DGL/PEG hydrogels prepared as described above. Control non-porous 2/25 and 2/37 mM DGL/PEG hydrogels were prepared as follows: DGL in PBS were placed in the first compartment of a dual-chamber syringe and PEG-NHS with PBS in the other compartment to obtain 300 μL in each cartridge. The dual-chamber syringe connected to a mixing nozzle was placed in a Texture Analyzer TA.HDplus (Texture Technologies, Hamilton, MA) and the force needed to push the plunger while maintaining a 2 mm/s velocity was recorded using a 500 kg-load cell. Distillated water was tested as a positive control.

2.6. Hydrogels characterization

2.6.1. Dynamic mechanical analysis

Non-porous (2 × 9.1 mm) and porous hydrogel discs (3 × 9.1 mm) of various compositions (DGL/PEG and Gaa:Pc molar ratio) were analyzed by cyclic compression with a dynamic mechanical analyzer (DMA 242 E Artemis, NETZSCH, Germany). Hydrogels domain of linearity was first determined with a strain sweep test in compression performed in PBS immersion, at room temperature. Samples were then subjected to compression at 10 % and 30 % strain (for non-porous and porous hydrogels respectively) with amplitudes of 50 μm and frequency of 1 Hz in PBS immersion at a constant 25 ˚C temperature.

2.6.2. Swelling ratio measurements

The swelling ratio (Qs) of 2 mm thick and 9 mm diameter half circle hydrogels was determined in PBS at 37 ˚C from non-porous hydrogels. Briefly, hydrogels were immersed in nitrogen and freeze-dried (Cosmos, Cryotec) for 48 h at 400 mTorr. Freeze-dried samples were weighed using an analytical balance, immersed in a 37 ˚C PBS solution and kept at 37 ˚C. Samples were weighed using analytical balance after 1;2;4;8; 24 and 48 h of immersion. Measurements were taken until reaching equilibrium. The swelling ratio was calculated using the following equation:

$$Qs = \frac{Ws - Wd}{Wd}$$

Where Ws represents the swollen weight of the sample at time t and Wd represents the dry weight of the freeze-dried sample.

2.6.3. Gel fraction

The gel fraction was measured to evaluate the extent of network formation. Drops of 200 μL of hydrogel precursors were prepared with various concentration of DGL/PEG, pluronic® F-68 and Gaa:Pc molar ratio. Briefly, the mass of non-porous hydrogels was recorded for each specimen after freeze-drying (Cosmos, Cryotec) for 24 h, and after incubation in ultrapure water at room temperature for 24 h and freeze-drying, until a constant mass and an equilibrium was reached. The final weight divided by the initial freeze-dried weight without the mass of salts was then expressed as gel fraction, in percentage.

2.6.4. Porosity characterization

Porosity characterization was performed on EPH cylinders produced as described above (injected or with manual homogenization) using fluorescein-labelled DGL (DGL-FITC) at 0.4 % of the final DGL concentration. Their structure was quantified by image analysis from 400 μm z-stacks made by laser scanning confocal microscopy imaging (LSCM Zeiss Imager.Z2) in PBS immersion. A stack was performed on both sides of three 2-mm high cylinders per hydrogel leading to 6 stacks/hydrogel. At least three hydrogels/condition were prepared for characterization at three different time points.

2.7. In vitro characterization

2.7.1. Cytotoxicity of non-porous hydrogels extracts

Non-porous 2/25 mM DGL/PEG hydrogel drops were formulated with Gaa:Pc at a final concentration of 1.1 M and 1.33:1 and 1.75:1 molar ratios or with pluronic® F-68 at 1.7 and 5 %. Immediately after formulation and without washing, 2/25 mM DGL/PEG hydrogel drops were immersed in 0.5 mL culture medium (Dulbecco's Modified Eagle Medium (DMEM) F-12 supplemented with 10 % fetal bovine serum

(FBS) and 1 % Penicillin/Streptomycin (P/S), Thermo fisher scientific) for 24 h at 37 °C and 5 % CO_2. In parallel, normal human dermal fibroblasts (NHDF, Promocell) were seeded on 24 wells plate at a density of 2000 cells/cm^2 and grown in culture medium at 37 °C with 5 % CO_2. After 24 h, culture medium was removed and cells were immersed in a 1 mL mix of culture medium and 24h-hydrogels-extracts at a ratio 1:1 or in a mix of the acid:base ratio and culture medium at a ratio 1:1 as control. Cell proliferation was assessed by an alamar® blue assay (Thermo fisher scientific) after 48 h in contact with 24h-hydrogel-extract or acid:base solutions of various molar ratio as follows: the culture medium was removed, cells were washed with Dulbecco phosphate buffered saline (DPBS, Gibco) and immersed in 400 µL of a 10 % alamar® blue mix in culture medium. After 3 h of incubation at 37 °C, 5 % CO_2, the supernatants were harvested and their fluorescence measured with a fluorescence microplate reader (TECAN infinite® 200) at excitation 535 nm and emission 610 nm.

2.7.2. EPH cytocompatibility

EPH of various conditions (1.6/25; 2/25 and 2/37 mM DGL/PEG) with Gaa:Pc at 1.1 M and 1.33:1 molar ratio and 3.3 % pluronic® F-68 were injected inside 2 mL conical tubes under sterile conditions to obtain 2 mm high cylinders as described above. Directly after formulation and cutting, and without any washing or post-formulation treatments, EPH cylinders were transferred into non-cell-treated 24-well plates (Corning). 5×10^4 NHDF were seeded onto non-washed EPH in 600 µL culture medium and incubated at 37 °C and 5 % CO_2. Culture medium was refreshed 24 h post seeding and every two days for 21 days. Cell viability was assessed by a live/dead assay after 6, 24 and 48 h in direct contact with EPH. Briefly, EPH containing cells were washed once with DPBS and 400 µL of a mix of propidium iodide and calcein (Thermo fisher scientific) at 6 and 1 µM respectively in DPBS was added to samples. After 20 min of incubation at 37 °C and 5 % CO_2, samples were observed by LSCM (Zeiss Imager.Z2) within 20 min (live cells excitation at 488 nm and emission at 509 nm, dead cells excitation at 561 nm and emission at 572 nm). The viability percentage was determined 24 h post seeding as the number of live cells on the total number of cells (dead and alive) on EPH. After 21 days, EPH containing cells were rinsed once with DPBS and fixed for 30 min with PFA 4 % (Thermo fisher scientific) at room temperature (RT) followed by DPBS extensive washing. Fixed EPH containing cells were used whole or manually sliced. Samples were permeabilized with 10 min' incubation in a solution of PBS and 0.1 % triton (Euromedex) and then immersed in blocking solution (5% goat serum) for one hour. Antibodies directed toward type I collagen (Novotec, dilution: 1/200) or toward fibronectin (Abcam, dilution:1/250) were applied on samples in goat serum 0.1 % for 2 h. Samples were then incubated with the secondary antibody (Abcam Alexa Fluor 647, dilution 1/500) for 2 h. For nuclear and actin counterstaining, whole cylinders or slices were incubated for 10 min in a mix of DAPI (5 µg/mL) and rhodamine-conjugated phalloidin (5 µg/mL) in DPBS. All incubations steps were performed at room temperature, samples were rinsed three time in DPBS between each step and imaged immersed in DPBS by LSCM (Zeiss Imager.Z2).

2.8. In vivo EPH biocompatibility

All procedures were carried out in accordance with the guidelines for ethical care of experimental animals of the European Community and approved by the Ethics Committee of Animal Experiments of French Ministry of Agriculture (CECCAPP-IBCP-2016-004, #8098). Seven-weeks old male hairless SKH1 mice (Charles River, Ecully) were anesthetized by intraperitoneal xylazin-ketamin injection. A small incision was performed at the lower back of the mice and two subcutaneous pockets were created with a sterile spatula along mice flanks. Various hydrogels conditions (1.6/25; 2/25 or 2/37 mM DGL/PEG) were injected (400 µL) directly into the subcutaneous pockets. Non-porous DGL/PEG hydrogels of various conditions in PBS were injected as control (500 µL). After hydrogel injection, the incision was sutured. EPH were made using a set Gaa:Pc 1.1 M concentration and 1.33:1 molar ratio and 3.3% pluronic® F-68. Mice, fed *ad libitum*, were monitored every two days for recovery and signs of distress. After three weeks, the mice were euthanized by anesthetic overdoses (intra-peritoneal injection of thiopental) and hydrogel samples were recovered with surrounding tissue. Samples were fixed with paraformaldehyde (PFA) in PBS at 4 % overnight at 4 °C, embedded in paraffin, sectioned and stained with Masson's trichrome using standard procedures. To highlight the penetration of blood vessels in the implanted hydrogels, sections were stained for type IV collagen (Novotec, France) by immunofluorescence, cell nuclei were counter-stained with 2 µg/mL DAPI solution and observed by confocal microscopy. Macrophages inside hydrogels were detected with antibodies against F4/80 (Novotec, France) by immunohistochemistry. The entire sample area with surrounding tissues was imaged at 3 various heights for each condition using a Zeiss Axio Scan Z1 for brightfield acquisitions and a LSCM (Zeiss Imager.Z2) for fluorescent acquisitions. Pore size after injection was quantified using the ZEN software at 2 various heights for each hydrogel. Three hydrogels per condition were quantified, accounting to an average of 300 pore diameter values for each condition.

2.9. Statistical analysis

Statistical analyses were performed with Graphpad prism. Tests were performed using variance analysis (ANOVA) after a Shapiro-Wilk normality test. Graphical data are presented as mean ± standard deviation (SD) and p-values of 0.05 and below were considered significant. Data values are presented as mean ± standard error (SEM). Each experiment was repeated at least 3 times.

3. Results

3.1. Adequacy and concomitancy of effervescence with DGL/PEG hydrogel crosslinking

A series of optimization and characterization studies on the interactions and suitability of effervescent reactions with DGL/PEG hydrogels crosslinking was first carried out to match both reactions and allow to select adequate effervescent components and range of compositions (Fig. 1). Since effervescent reactions can produce by-products that are involved in biological processes, such as coagulation (sodium citrate [37]) or skeletal muscle contraction (calcium ion [38]), an acid and base pair suitable for direct *in vivo* injection is mandatory. Hence, we selected glacial acetic acid (Gaa) and solubilized potassium carbonate (Pc) effervescent pair, as it only results in carbon dioxide, water and potassium acetate (an acidity regulator). Furthermore, upon mixing, this pair ensures a strong and long-term effervescence while avoiding ions re-precipitation. Logically, modifications of Gaa:Pc molar ratio allowed to control final solution's pH (Fig. 2A), which, in turn, drastically influenced the DGL/PEG hydrogel crosslinking. For instance, the time needed for a 2/25 mM DGL/PEG hydrogel to form a self-standing material was delayed to 350 s at acidic pH (5) while an alkaline pH (10) resulted in its immediate crosslinking (Fig. 2B). Therefore, to synchronize the effervescent reaction with the hydrogel formation, a range of Gaa:Pc molar ratios between 1.75:1 and 1.33:1, resulting in a final pH between 5.5 and 7.4, was found to be adequate by providing a crosslinking of the hydrogels within seconds to minutes, regardless of the hydrogel concentration used (Fig. 2C). Confirming a strong influence of the pH on DGL/PEG chemistry, unrelated to the concentration used and the presence of surfactant, final molarities of Gaa:Pc and concentrations of pluronic® F-68 did not play a role (Fig. 2D, E). The pH influence was further reflected in the efficiency of the chemical reaction between DGL and PEG, leading to hydrogel formation (Fig. 3A and B). When prepared

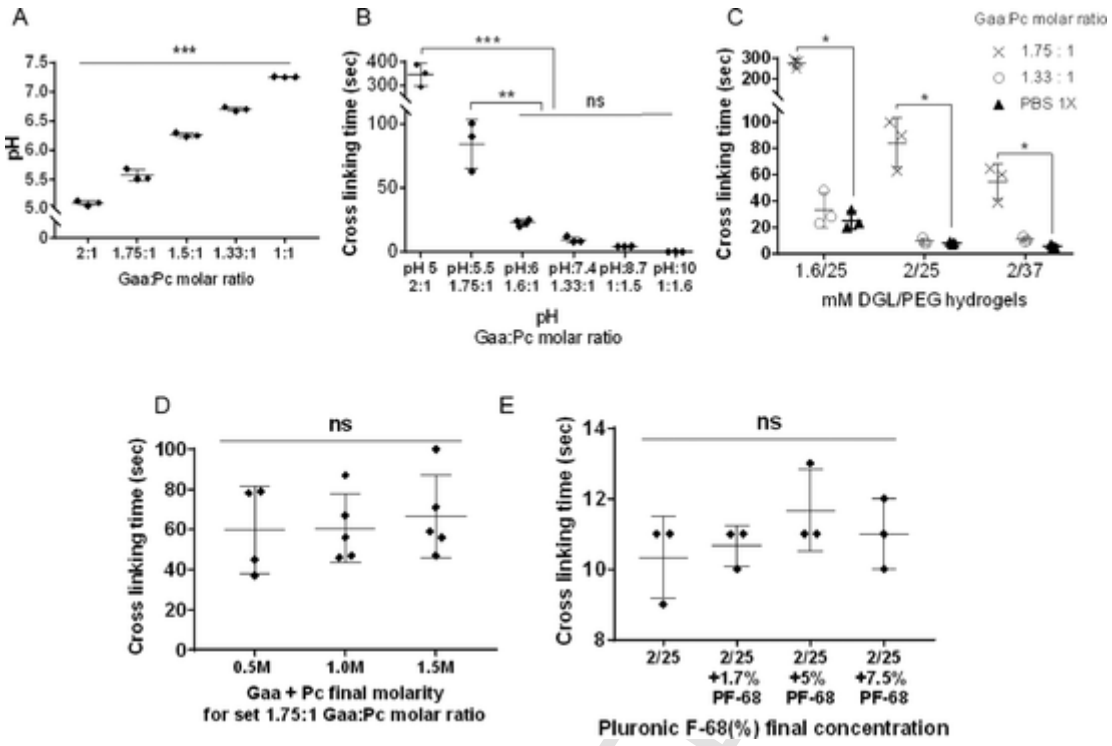

Fig. 2. Compatibility of effervescent reactions with DGL/PEG hydrogels. (A) pH of Gaa:Pc solutions right after effervescence as a function of Gaa:Pc molar ratio. (B) Influence of Gaa:Pc molar ratio on the time needed for a 2/25 mM DGL/PEG hydrogel to form a self-standing material. (C) Time needed to form self-standing hydrogel between various DGL/PEG concentrations, as a function of a range of Gaa:Pc molar ratio. (A), (B), (C): Gaa:Pc solutions used for a given 1.1 M final concentration. (D) Influence of Gaa: Pc final molarity on time needed to form a 2/25 mM DGL/PEG hydrogel for a given 1.75:1 Gaa:Pc molar ratio. (E) Influence of Pluronic® F-68 final concentration on time needed to form a 2/25 mM DGL/PEG hydrogel. (A) and (B) One-way Anova with Tukey's multiple comparison test. (C) Kruskal Wallis with Dunn's multiple comparison test versus PBS 1X. (D) and (E) Kruskal Wallis with Dunn's multiple comparison test. (B), (C), (D), and (E) the term "cross linking time (sec)" was used to refer as the time needed to form the self-standing material. Results presented as mean ± SD. Ns: no significance, *: $p < 0.05$, **: $p < 0.01$, ***: $p < 0.001$ - (at least $n = 3$ per condition).

in presence of Gaa:Pc, an increase of unreacted DGL (up to 2 folds) could be measured, as compared to a control 2/25 mM FITC-DGL/PEG hydrogel prepared in PBS (Fig. 3A), contrarily to the presence of pluronic® F-68 which did not have any influence (Fig. 3B). As a corollary, the hydrogel's mechanical properties, gel fraction and swelling properties were as well influenced by the final pH induced by the Gaa:Pc pair. Indeed, the complex modulus (E*) of all DGL/PEG non-porous hydrogels compositions, determined by mechanical dynamic analysis, showed a steep decrease of about 40 % and 30 % when prepared with 1.75:1 and 1.33:1 Gaa:Pc molar ratio, respectively (Fig. 3C). Nonetheless, the presence of Gaa:Pc at various ratios did not prevent to control the hydrogel bulk mechanical properties from 10 to 50 kPa, through the variation of DGL/PEG concentrations.

In line with the mechanical properties decrease, a decrease of the gel fraction was observed for hydrogels prepared with Gaa:Pc regardless of the hydrogel composition (Fig. 3E). The gel fraction was observed to decrease by respectively 18.7 ± 1.4 %, 10.3 ± 1.8 %, and 17.9 ± 0.9 % for 1.6/25, 2/25 and 2/37 mM DGL/PEG hydrogel formulated with Gaa:Pc at 1.75:1 compared with controls made in PBS. This demonstrates that the addition of Gaa:Pc at 1.75:1 molar ratio has an influence on the DGL/PEG hydrogel network formation. This was further confirmed by an increased swelling ratio of all hydrogels compositions prepared with Gaa:Pc (Fig. 3F). Further confirming a lack of interactions with the crosslinking reaction, the addition of pluronic® F-68 did not result in variations of mechanical and swelling properties or gel fraction (Figs. 3D, 3G and S1).

Overall, these results confirm the influence of effervescence, and more precisely the resulting pH, on DGL/PEG hydrogels. All measured properties of hydrogels prepared with more acidic solutions (crosslinking delay, higher level of unreacted DGL, stronger decrease of mechanical properties and higher swelling) are in agreement with a lower level of crosslinking.

However, by selecting the suitable ratios of Gaa and Pc dissolved in PEG and DGL precursor solutions, neither the effervescence reaction nor the hydrogels' crosslinking were hampered. The tolerance towards acid and alkaline components of the covalent reaction of NHS ester end groups at the extremities of PEG molecules with free amine groups available at the surface of lysine dendrigrafts allows the crosslinking reaction to occur upon mixing while rapidly entrapping the produced gas (Fig. 4A and video S1).

3.2. Design and characterization of porous and injectable DGL/PEG hydrogels

Confirming our hypothesis, the successful entrapment of stabilized CO_2 bubbles in solid hydrogels ultimately result in pore formation. Logically, the resulting foamy structures showed an important volume expansion of 600 %, 500 % and 200 % for 1.6/25, 2/25 and 2/37 mM DGL/PEG hydrogels respectively, due to the effervescent reaction (Fig. 4B). An advantage of using two sole precursor solutions is to allow injection of the effervescent formulations with a commercial dual-chamber syringe system combined with a static mixer (Video S2). The strength needed on the plunger to inject non-porous and porous DGL/PEG hydrogels was close to that of water, confirming that hydrogel precursors are still in liquid form during injection (Fig. 4C).

After injection and within the range of Gaa:Pc molar ratio targeted, an open pore structure was formed after removal of the entrapped CO_2 bubbles, regardless of their compositions (Fig. 4D,E). The use of effervescence inside DGL/PEG hydrogels allowed to form a porosity comprised between 75.0 % ± 2.3 % and 79.7 % ± 1.9 % with an average

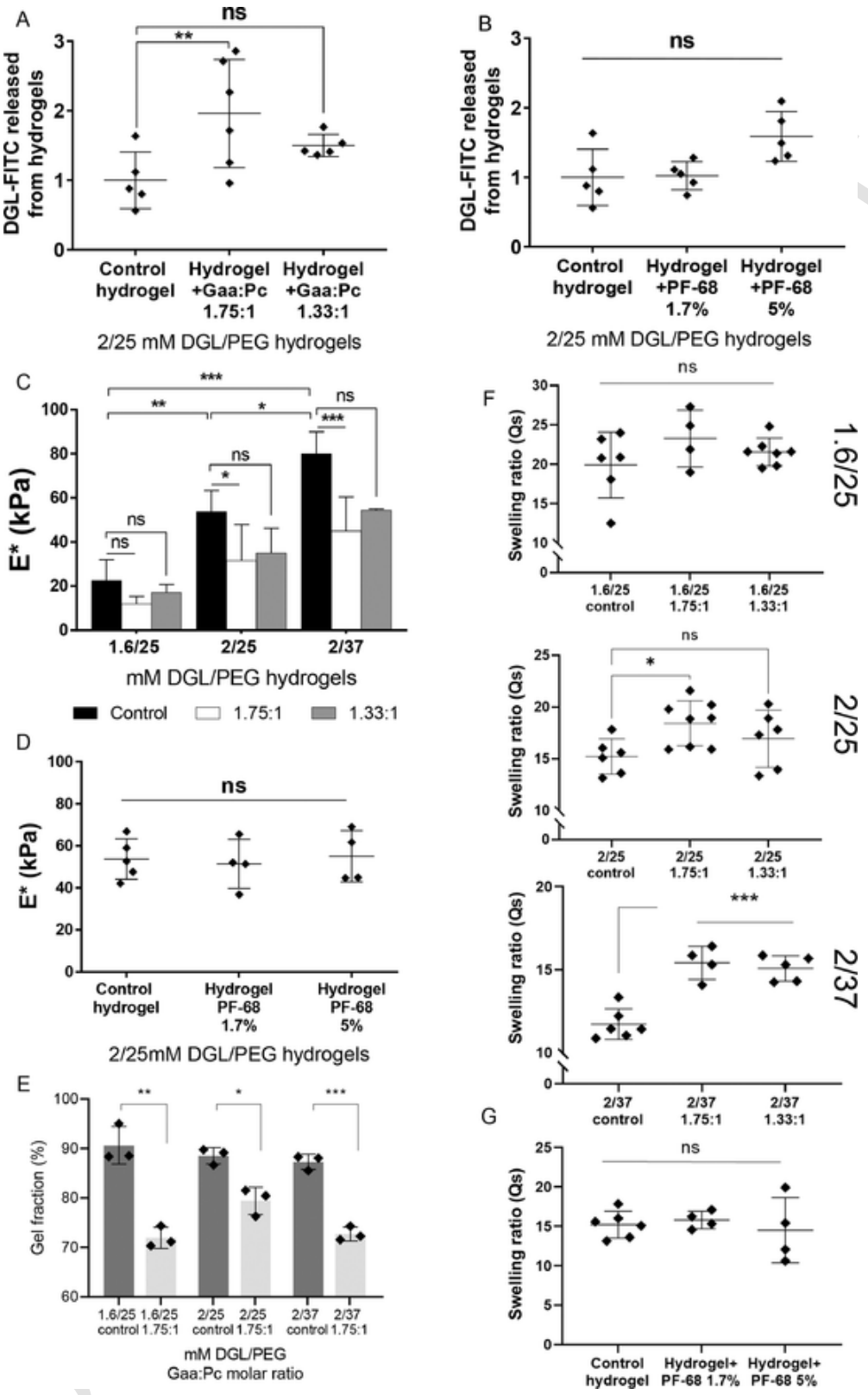

Fig. 3. Influence of pH induced by effervescence on non-porous DGL/PEG hydrogels. (A), (B) DGL-FITC release from non-porous 2/25 mM DGL-FITC/PEG hydrogels formulated with (A) various Gaa:Pc molar ratios at a final 1.1 M concentration or with (B) various pluronic® F-68 concentrations. The fluorescent signal is normalized to the one of control hydrogels (formulated in PBS 1X). (C), (D) Complex modulus (E*) in kPa of various non-porous hydrogel conditions formulated in PBS 1X (control) or with (C) 1.75:1 and 1.33:1 Gaa: Pc molar ratio at 1.1 M final concentration or (D) with pluronic® F-68 at a final 1.7% and 5% concentration. (E) Gel fraction of DGL/PEG hydrogels of various concentration formulated in PBS or with Gaa:Pc at 1.1 M and 1.75:1 molar ratio. (F), (G) Swelling ratio at equilibrium (48h post rehydration) of various DGL/PEG hydrogels formulated in PBS (control) or with (F) 1.75:1 and 1.33:1 Gaa:Pc molar ratio at 1.1 M final concen-

◀ tration or of a (G) 2/25 mM DGL/PEG hydrogel formulated with various pluronic® F-68 concentrations. One-way Anova + Dunnett's vs control hydrogel. Results presented as mean ± SD. Ns: no significance, *: $p < 0.05$, **: $p < 0.01$, ***: $p < 0.001$, (at least n = 3 per condition), (E) t-test control hydrogel vs hydrogel formulated with Gaa:Pc at 1.75:1 molar ratio.

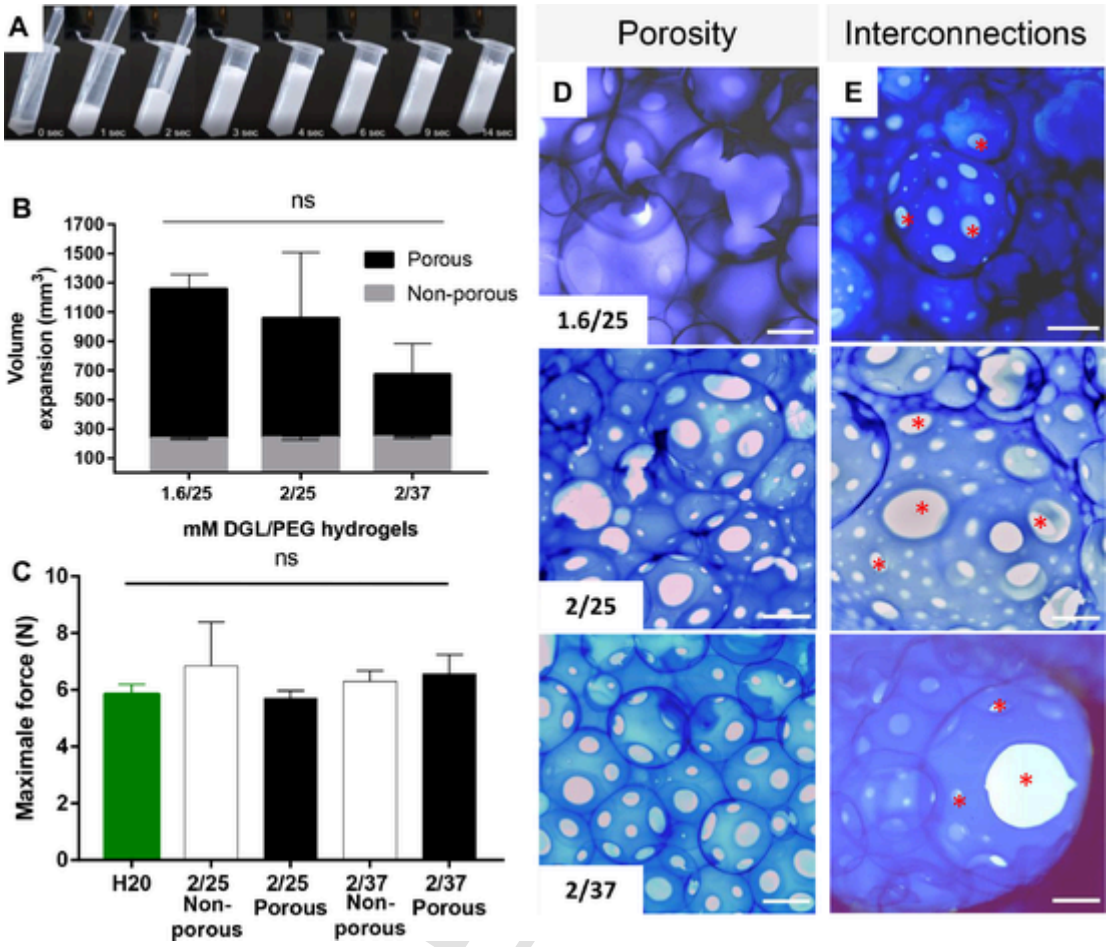

Fig. 4. (A) Time lapse of the volume expansion generated by the effervescence simultaneous to a 2/25 mM DGL/PEG hydrogel crosslinking reaction. (B) Calculation of volume expansion during formulation of porous VS non-porous 1.6/25; 2/25 and 2/37 mM DGL/PEG hydrogels. (C) Strength applied on dual-chamber syringe plunger to maintain a 2 mm/s injection speed to inject H_2O (positive control) non-porous and porous 2/25 mM DGL/PEG hydrogels. (D), (E) Coomassie blue staining of effervescent porous hydrogels to show (D) porosity obtained within 1.6/25, 2/25, and 2/37 mM DGL/PEG hydrogels and (E) windows of interconnection in a 2/25 mM DGL/PEG hydrogel (red star: one window of interconnection) scale bar 400 μm. Hydrogels formulated with 1.33:1 Gaa:Pc molar ratio and 1.1 M final concentration and 3.3% pluronic® F-68 . One-way Anova + Tuckey multiple comparison. Results presented as mean ± SD. Ns: no significance, *: $p < 0.05$, **: $p < 0.01$, ***: $p < 0.001$, ($n = 3$ per condition) (For interpretation of the references to color in this figure legend, the reader is referred to the web version of this article.).

pore size between 280.1 ± 54.9 μm and 313.0 ± 32.3 μm (Fig. 5A, B, Table 1 and video S3,). Reflecting the entrapment of the CO_2 bubble population, the pore sizes were characterized by a broad distribution (35 to 3000 μm), the most abundant fraction being comprised between 50 and 100 μm (Fig. 5B).

Strikingly, windows of interconnection were visible between pores. They are the voids linking one pore to another, enabling to form a pathway inside the hydrogel network. From 1 to 50 windows of interconnection per pore were observed throughout the entire construct, regardless of the composition of the hydrogels. Similarly to pore distribution, the numerous windows of interconnection between pores were broadly distributed for all injected hydrogels, with average diameters spanning from 100.7 ± 14.9 μm to 131.4 ± 12.9 μm and population mode comprised between 10 and 30 μm (Fig. 5C and Table 1).

Neither the DGL/PEG concentration, the Gaa: Pc ratio, nor the pluronic® F-68 percentage significantly influenced the hydrogels' pores and interconnection sizes, supporting the possibility to vary the stiffness of the support without impacting the resultant porosity (Table S1). However, lower porosities were obtained with lower amounts of pluronic® F-68 and acidic Gaa:Pc ratios, suggesting that a threshold concentration and molar ratio is needed to have homogeneous porosity. The use of a dual-chamber syringe to homogenize the precursor solutions interestingly resulted in bigger pores than manual mixing, which provides perspectives on a possible porosity modulation through way of delivery.

Since mechanical properties are dependent on the porosity generated inside the material, the mechanical properties of non-porous versus porous hydrogels were studied. The porosity induced by the effervescent reaction logically reduced the overall mechanical properties by respectively 37 % to 49 % for porous 2/25 and 2/37 mM DGL/PEG hydrogel, compared with their non-porous counterparts (Fig. 5D). However, in our system, both the composition in DGL/PEG and the chosen Gaa: Pc molar ratio allowed EPH mechanical properties modulation from 12.7 ± 0.9 to 29.9 ± 1.7 kPa while forming a self-standing material (Figs. 5E and S2). This versatility combined with the highly interconnected porosity is an asset to meet the requirements of various tissue engineering and regenerative medicine applications [39,40].

Cytotoxicity and cytocompatibility of effervescent porous hydrogels

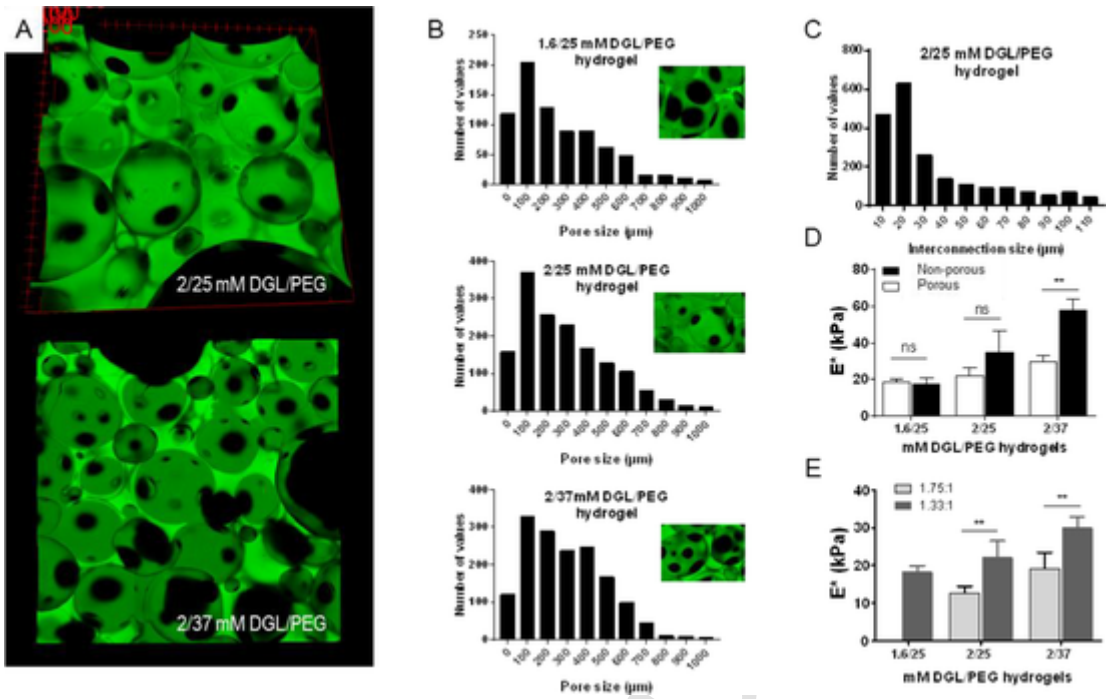

Fig. 5. Porosity characterization of various effervescent porous hydrogel (EPH) made by injection. (A) Representative picture of 2/25 and 2/37 mM FITC-DGL/PEG effervescent porous hydrogels (EPH). (B) Pore size of various FITC-DGL/PEG EPH compositions and (C) windows of interconnection size of 2/25 mM DGL/PEG EPH, formulated with 1.33:1 Gaa: Pc molar ratio at 1.1 M and 3.3% Pluronic® F-68 by injection. (D) Complex modulus (E*) in compression of non-porous vs porous DGL/PEG hydrogels of similar composition (i.e. Gaa: Pc molar ratio at 1.33:1 and 1.1 M final concentration and Pluronic ® F-68 at 3.3%). (E) Complex modulus (E*) in compression of various DGL/PEG EPH formulated with 1.33:1 or 1.75:1 Gaa: Pc molar ratio and 3.3% pluronic® F-68. t-test (D) non-porous versus porous hydrogels and (E) EPH formulated with Gaa: Pc at 1.75:1 versus 1.33:1 molar ratio. Results presented as mean ± SD. Ns: no significance, *: $p < 0.05$, **: $p < 0.01$, ***: $p < 0.001$, (at least n = 3 per condition).

Table 1
Comparison of the resultant porosity created in various EPH compositions: 1.6/25, 2/25 and 2/37 mM DGL/PEG with a set 1.33:1 Gaa:Pc molar ratio at 1.1 M and with pluronic F-68 concentration set at 3.3%. The porosity was made by injection through the dual-chamber syringe. No significant differences were reported between conditions (One-way Anova + Tukey's multiple comparison test, n = 3 hydrogels per condition).

Parameter studied	Porosity characterization		
Hydrogel concentration mM DGL/PEG	Pore Size (µm) -**Mean ± SEM** [Mode] - Median	% Porosity	Size of windows of interconnection (µm) -**Mean ± SEM** [Mode] - Median
1.6/25	**280.1 ± 54.9** [50-100] -203	75.0 ± 2.3	**100.7 ± 14.9** [10-20] - 38
2/25	**307.2 ± 36.5** [50-100] -243	76.8 ± 1.4	**130.4 ± 21.2** [20-30] – 44
2/37	**313.0 ± 32.3** [50-100] -272	79.7 ± 1.9	**131.4 ± 12.9** [20-30] - 93

Since the porous hydrogel is formed through an effervescent reaction, the potential toxicity of the effervescence by-products was initially evaluated with normal human dermal fibroblastic cells (NHDF). Cells exposed to 24h-extracts of effervescent hydrogels indicated a significant decrease of metabolic activity compared to similar hydrogels prepared without effervescent components, regardless of the Gaa:Pc concentrations employed (Fig. 6A). This decrease was not related to the presence of pluronic® F-68 surfactant (Fig. 6C) but appeared linked to the acid/base couple employed, as was observed when Gaa:Pc was added directly onto NHDF at the same concentration (Fig. 6B). However, NHDF placed directly in contact with unwashed EPH showed cellular adhesion, which was assessed after 6 h and confirmed after 48 h through clear cellular spreading (Fig. 6D). Strikingly, NHDF were 72 ± 4%, 88 ± 3% and 85 ± 2% viable after 24 h on 1.6/25, 2/25 and 2/37 mM DGL/PEG EPH respectively, without any washing or post-formulation treatment, demonstrating that neither the acid/base couple nor the CO_2 bubbles were harmful to cells (Fig. 6E). Cell viability on unwashed EPH was not different from their extensively washed counterparts used as positive controls, confirming the non-cytotoxicity of the formulations described here, and demonstrating the potential of EPH to be used in direct *in vivo* injection.

It was also observed that by varying the DGL/PEG composition of EPH, cells behaviour in terms of early adhesion and cell spreading could be varied (Fig. 6F). Soft conditions (i.e. 1.6/25 mM DGL/PEG) resulted in less spread cells than stiffer ones (i.e. 2/25 and 2/37 mM DGL/PEG).

The effect of DGL/PEG mechanical and biochemical versatility on cells [35] was thus preserved in the EPH settings.

Aside cytotoxicity, cytocompatibility of the porous hydrogels is an equally crucial property for any potential tissue engineering and regenerative medicine applications [41], which require cell survival, adhesion and proliferation within the hydrogels' pores to allow the formation of a new tissue. DAPI/fluorescent phalloidin staining of NHDF cells showed a homogeneous distribution throughout 2 mm-thick hydrogel after 24 h (Fig. 7A), indicating a rapid entry within the hydrogel pores, due to the highly interconnected porous architecture. NHDF effectively covered a major part of the available inner surface and began to fill the porous structure and create a network of cells 21 days post seeding, attesting their ability to proliferate inside the EPH (Fig. 7B). Finally, EPH allowed *in vitro* deposition of extracellular matrix (ECM) proteins, such as fibronectin and type I collagen, for all tested conditions (Fig. 7C).

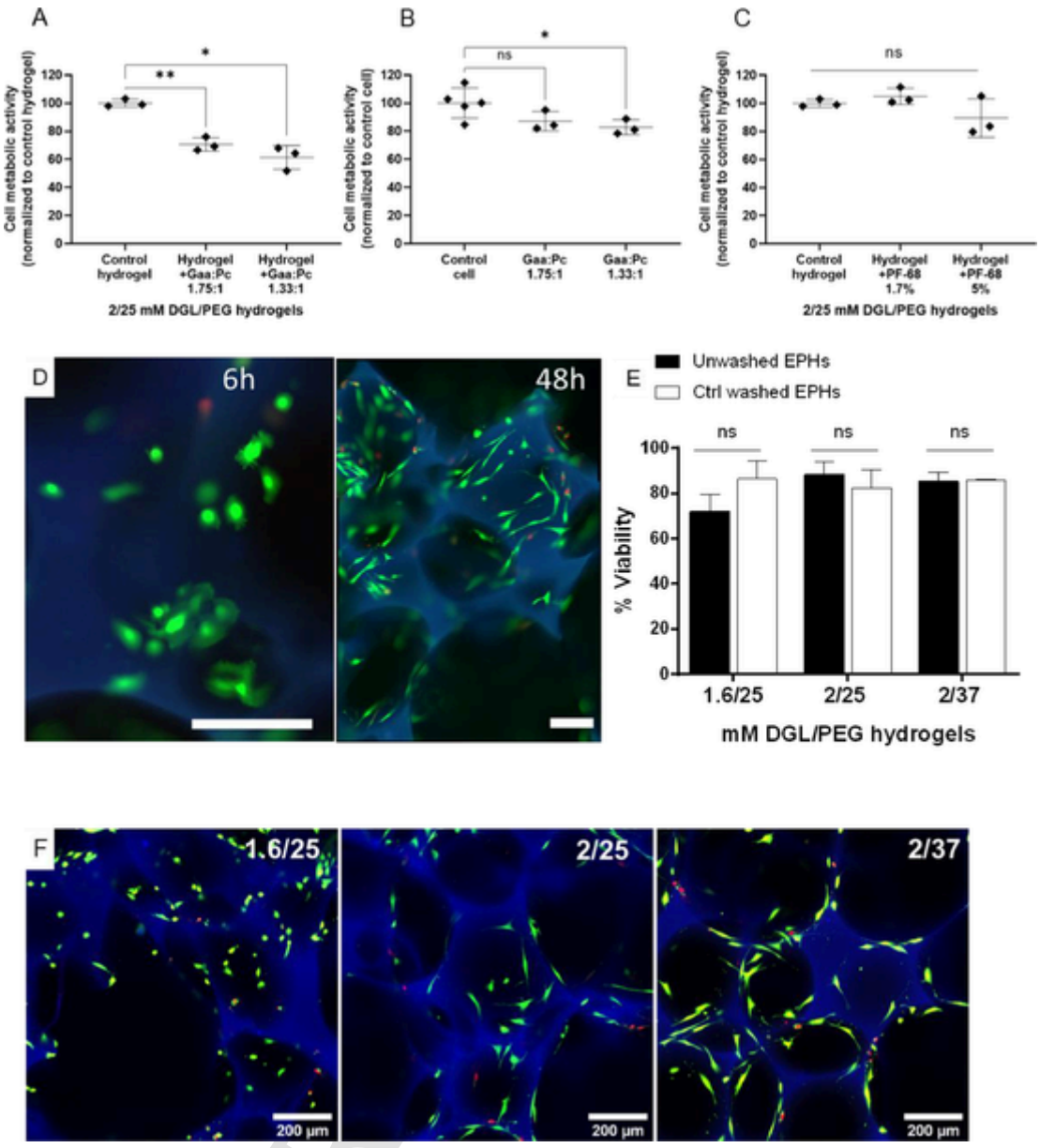

Fig. 6. *In vitro* EPH suitability for direct *in situ* injection purposes: cytotoxicity. (A) NHDF metabolic activity after 48 h in contact with 24h-extract of non-porous 2/25 mM DGL/PEG hydrogels formulated with various Gaa: Pc molar ratios at 1.1 M. (B) NHDF metabolic activity after 48 h in contact with only Gaa: Pc molar ratios at 1.1 M or (C) with 24h-extract of non-porous 2/25 mM DGL/PEG hydrogels formulated with various pluronic® F-68 concentrations. (A), and (C) are presented as the overall fluorescence normalized to that of the control hydrogel. (B) is presented as the overall fluorescence normalized to that of the control cells. (D) Live/Dead assay of NHDF cells in direct contact with EPH, 6 and 48 h post seeding (live cells represented in green and dead cells in red, the hydrogel is represented in blue, 6h, scale bar: 50 µm, 48h, scale bar: 200 µm). (E) Quantification of live cells versus the total number of cells after 24 h on 1.6/25, 2/25 and 2/37 mM DGL/PEG EPH used immediately after formulation, without any washing or post-formulation treatment, versus cells on washed EPH of the same conditions as control. (F) Live/dead assay on EPH of various compositions showing various cell spreading 24 h post seeding. (A), (B), (C): One-way Anova + Dunnett's vs control hydrogel or control cells. E: t-test unwashed EPH versus washed EPH (control). Results presented as mean ± SD. Ns: no significance, *: $p < 0.05$, **: $p < 0.01$, ***: $p < 0.001$, (n = 3 per condition) (For interpretation of the references to color in this figure legend, the reader is referred to the web version of this article.).

3.2.1. In situ injectability and biocompatibility of effervescent porous hydrogels

Since the important hydrogels' pores interconnection allows cells to infiltrate and colonize the entire porous structure *in vitro*, tissue ingrowth inside *in vivo* formed porosity was evaluated by EPH subcutaneous injection in the back of mice (Fig. S3A and video S4). Immediately after initiating the injection, an important volume expansion was visible due to the effervescent reaction and CO_2 bubble formation. In less than a minute, hydrogel crosslinking was sufficient to remove the syringe, leaving a porous implant in place. The injected material was excised after 3 weeks, during which no evidence of sepsis, infection or pain were detected on the animals. Upon excision of the injected implants, EPH were visibly of darker and more reddish coloration than their non-porous counterparts (Fig. S3B). Staining with Masson's trichrome clearly revealed the porous structure within the injected EPH as well as a mild foreign body reaction with the formation of a fibrous capsule surrounding both non-porous and porous hydrogels (Fig. 8). The porous structure formed directly *in vivo* exhibited a decreased pore size compared with hydrogels injected in tubes (Fig. S4). However, the compatibility of the resultant effervescent porous structure to sustain cellular infiltration and tissue formation was indicated by the presence of cells (nuclei in purple and cytoplasm in light purple) and neo-tissues

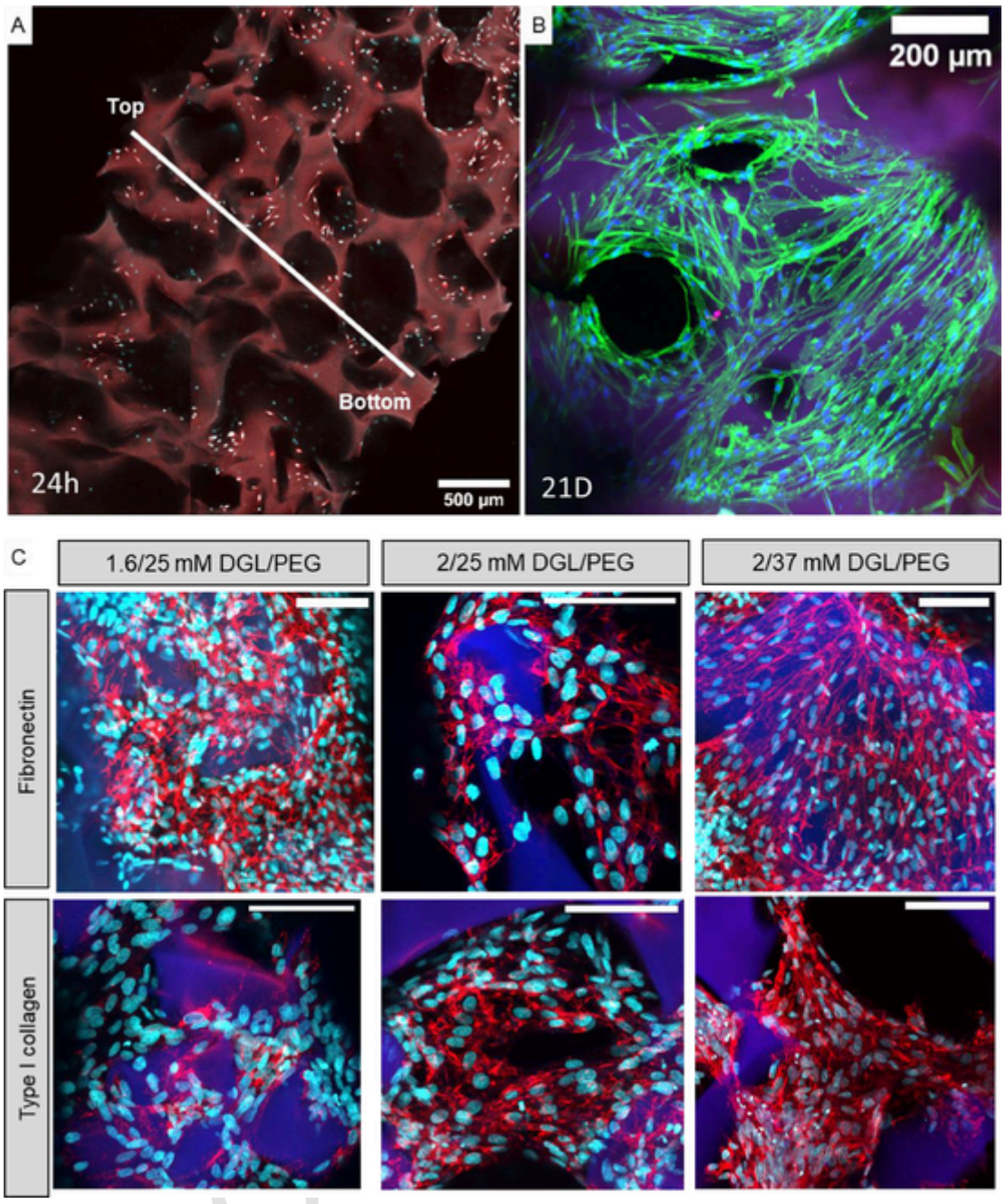

Fig. 7. *In vitro* EPH suitability for direct *in situ* injection purposes: cytocompatibility. (A) Cellular distribution throughout a 2/25 mM DGL/PEG EPH 24 h post seeding by DAPI/Phalloidin staining (cell nuclei in cyan, actin cytoskeleton in red and hydrogel in pink). (B) Cellular morphology and pores filling after 21 days of culture inside a 2/25 mM DGL/PEG EPH (cell nuclei in blue, actin cytoskeleton in green and hydrogel in purple). (C) ECM deposition by cells 21 days post seeding in various EPH compositions (cell nuclei in cyan, fibronectin and type I collagen deposition in red, hydrogel in blue). Scale bar 100 µm (For interpretation of the references to color in this figure legend, the reader is referred to the web version of this article.).

within the hydrogels (collagen deposits in green). Cells with elongated nuclei and light cytoplasm, presumably fibroblasts, were visible within the hydrogel in close contact with collagen. This cellular infiltration and collagen deposition were promoted despite the formation of a fibrous capsule surrounding the hydrogel (highlighted with the black dotted line). These results clearly indicate that the hydrogel was well integrated by tissues and was not isolated by the fibrous capsule. On the contrary, non-porous hydrogels did not exhibit any porosity aside from the void path created by the mixing nozzle (Fig. 8B). Similarly to EPH, non-porous hydrogels were surrounded by a fibrous capsule made of fibroblasts and collagen deposition. However, contrarily to their porous counterparts, non-porous hydrogels exhibited a too tight network to allow cells to enter the structure, confining them to hydrogel rims. They thus showed no tissue deposition apart from the fibrous capsule.

Aside fibroblasts-like cells, various cell populations could be distinguished inside EPH, among which a low density of inflammatory cells (granulocytes or lymphocytes) and macrophages, concentrated at the rim, with evidence of hydrogel phagocytosis (blue close-ups Fig. 8B). A specific staining for macrophages confirmed their slight presence inside the injected EPH, underlining a mild inflammatory reaction (Fig.S5). Cellular migration inside the hydrogel with low presence of inflammatory cells indicated the porous formulation has no harmful effect on cells and surrounding tissues.

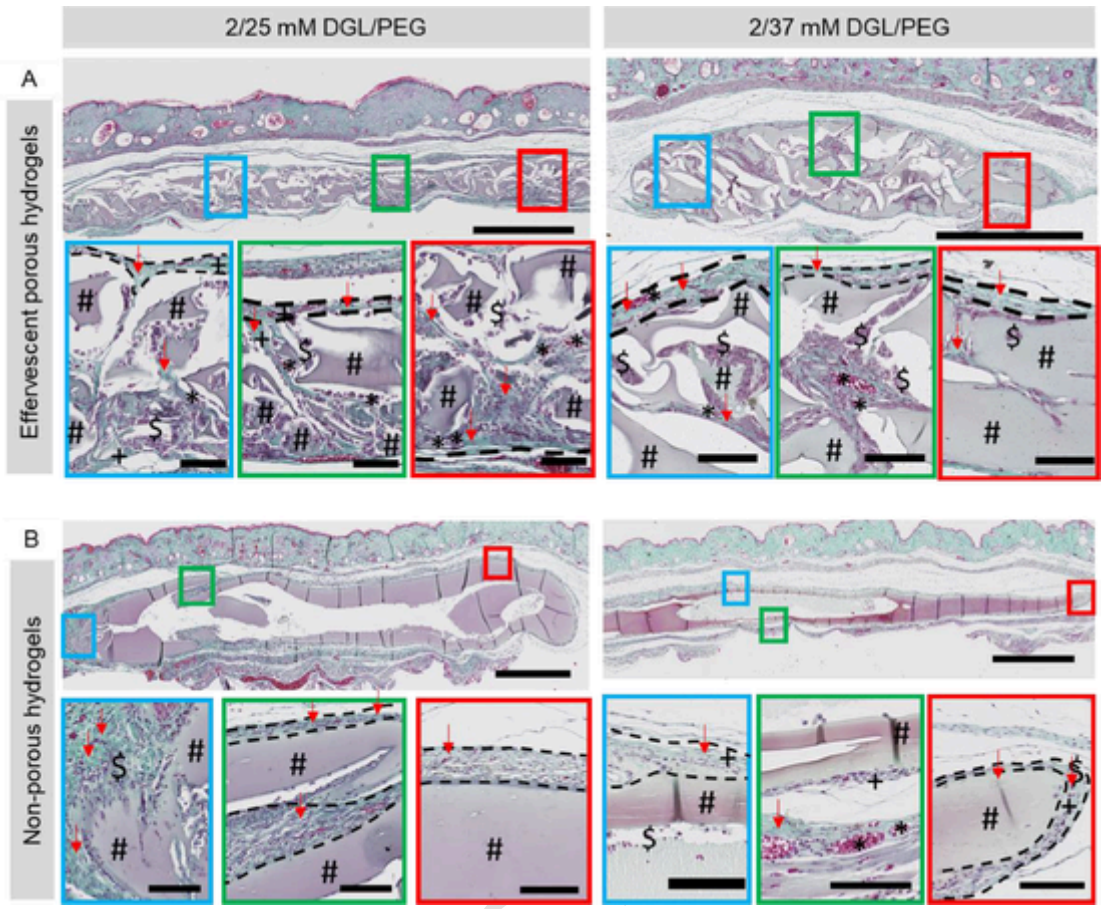

Fig. 8. EPH and non-porous DGL/PEG hydrogels directly injected in subcutaneous pockets on the back of mice. (A), (B) Masson's trichrome staining of the full explants after 3 weeks implantation and close-ups highlighting hydrogel (#), the fibrous capsule (black dotted line), macrophages ($), synthetized collagen (in green, red arrow), fibroblasts (+) and blood vessels (*). Cell nuclei appear in purple and cytoplasm in light purple. (A) Porous hydrogel of various compositions (2/25 and 2/37 mM DGL/PEG) formulated with 1.33:1 Gaa:Pc molar ratio at a final 1.1 M and 3.3 % pluronic® F-68. (B) Non-porous DGL/PEG hydrogels of various compositions (2/25 and 2/37 mM DGL/PEG) formulated in PBS 1X. Scale bar whole explant 1 mm, scale bar close up: 100 μm (For interpretation of the references to color in this figure legend, the reader is referred to the web version of this article.).

In the injected EPH, an extensive vascularization could be observed within the pores throughout the entire hydrogel thickness (Fig. 8A), which was further confirmed with a specific staining for type IV collagen (Fig. S6). These results confirm that the porosity is well interconnected and sufficiently large to sustain vascular infiltration. On the contrary, no vascularization was visible inside non-porous control hydrogels. This observation further confirms the requirement of an adequate porosity to enhance neovascularization of hydrogels.

Of note, no gas cavity was observed after implantation demonstrating the absence of deleterious effect of the CO_2 bubbles on surrounding tissues.

4. Discussion

This is the first time that an effervescent approach has been used to develop a straightforward and injectable hydrogel that allows both pore formation and *in situ* delivery. The reaction of carboxylic acid and carbonate base to produce CO_2 bubbles is known since the 30's, and has been successfully and extensively used to produce effervescent tablets. The ease of this method, the lack of organic solvent and the cell biocompatibility of CO_2 [25] have logically prompted biomedical researchers to explore the potential of effervescently-produced CO_2 bubbles as porogens in hydrogels [29,30,32,33,42,43]. However, all previous attempts have never considered their potential for direct *in situ* injection and pore formation. Our data demonstrate that the DGL/PEG hydrogel, with controllable and swift polymerization in aqueous solutions, is sufficiently versatile to allow the effervescent reaction to occur while rapidly entrapping the produced gas to form porous hydrogels upon mixing. This rapid crosslinking is possible through the highly tunable reaction of NHS ester end groups at the extremities of PEG molecules with free amine groups available at the surface of lysine dendrigrafts. By taking advantage of the fast-setting DGL/PEG hydrogel, we bring closer the potential of porous hydrogels for tissue engineering applications and their practical use in clinical settings.

However, similarly to other crosslinking reactions that can be significantly disturbed or boosted by pH [44,45] the concomitancy of hydrogel formation and effervescent reaction relies in part on the pH sensitivity of the PEG and DGL polymerization. At acidic pH the NHS function on PEG molecules is less likely to undergo hydrolysis but is also less reactive, while at alkaline pH the function is more reactive but less stable [46]. Similarly, the α-amino group (pKa 9.16) and ε-amine (pKa 10) present at the DGL surface are not equally available at acidic or alkaline pH [47]. As a result, the DGL/PEG hydrogel crosslinking is delayed and less complete in acidic conditions, as demonstrated by a significant increase of unreacted DGL release from such hydrogels, a decrease of their mechanical properties and an increased swelling. Particularly, the decreased gel fraction observed in hydrogels formulated with acid:base at a 1.75:1 molar ratio compared with hydrogels formulated in PBS demonstrates that the pH influences the network formation of the hydrogels. This behavior is exploited here to orchestrate and match the reactions of effervescence and crosslinking of different DGL/PEG hydrogels via the carboxylic acid and carbonate base pair ratio. Contrarily to

acid and base pair, the presence of pluronic® F-68 in the resulting effervescent porous hydrogels (EPH) had no quantifiable effect on DGL/PEG hydrogels chemistry but was mandatory to stabilize the effervescence during crosslinking, especially for slow-setting hydrogels (i.e., 1.6/25 and 2/25 mM DGL/PEG).

Therefore, thought the careful optimization of effervescence parameters, we obtain a spontaneous and interconnected porosity, remnant of the produced bubbles entrapment inside the simultaneously generated DGL/PEG network. As a result, this straightforward method to induce a porosity inside tunable DGL/PEG hydrogels further allows tailoring of its mechanical properties through the choice of acid and base molar ratio used.

The characteristics of porosity in a hydrogel play a major role for the promotion of angiogenesis, to guide cellular fate inside the scaffold, and for a successful host tissue ingrowth, especially for large implants, since cell infiltration, proliferation, migration and differentiation is dependent on pore size and interconnection [25,48–50]. In our formulations, the porosity obtained is well in line with other systems using effervescence in non-injectable settings [30,31,45,51]. There is no clear consensus on a universal optimized pore size that could be suitable for all tissue-engineering applications [52]. For instance, fibrous or unmineralized tissues grow better in pores with size comprised between 10 to 100 μm while osteoblasts regenerate mineralized bone in larger pores (100-200 μm) [53,54]. However, the macroporosity herein described allows targeting a broad range of potential tissue engineering applications, such as myotube formation and skeletal muscle regeneration [55,56], osteoblast infiltration and mineralization [57,58], chondrocyte proliferation and cartilage ECM production [59] or vessel infiltration [14,60].

In addition to pore size, the interconnection between pores has been shown to be particularly relevant for many tissue engineering applications as a pathway between pores is required to provide the space for tissue to grow. Both cellular and vascular infiltration need to be enhanced inside porous hydrogels as they participate in tissue ingrowth. In our case, the produced pores are highly interconnected throughout the entire construct forming a continuity between pores. Such interconnection can be attributed to the explosive effervescence, which leads to a high density of bubbles in close contact with each other, and to the surfactant that stabilizes CO_2 bubbles and allows their local fusion [61,21]. This was related in our system to a relevant number of high-diameter windows of interconnection per pore. While the size of windows of interconnection plays an important role in neo-vascularization inside implanted scaffolds [62–64] the number of interconnections per pore is of particular relevance to increase tissue invasion [65] further consolidating the potential of the created porosity for tissue engineering applications.

As previously emphasized, the porosity is paramount to guide cell fate and tissue ingrowth. Therefore, its modulation could provide an interesting tool to meet the requirements of specific tissues. In this work, we highlighted that the homogenization method affected pore size without influencing the pathways between pores. Future work could thus focus on homogenization process through various static mixers to control the porous structure and thus influence cell behavior and tissue formation.

Regardless of the porosity created, any material that is aimed to be injected in the body must not induce any significant toxicity, either on cells or on the surrounding host tissue [66,67]. Moreover, they should not trigger excessive inflammation to allow correct tissue formation [68,69]. In our system, the DGL/PEG crosslinking modifications caused by the effervescent conditions result in a slight decrease of cell metabolic activity when cultured in contact with extracts from non-porous hydrogels. In addition to the effect of acidic pH on cells, the pH-related decrease of polymerization and resulting unreacted-DGL release could also account for this observation, since DGL becomes cytotoxic above a concentration of 5 μg/mL [36]. However, in the case of injected effervescent porous hydrogels, the DGL is sufficiently sequestrated inside the network to prevent cell mortality in direct contact. As a result, the inherent cell-interaction properties of the DGL/PEG hydrogels (brought by the DGL amine residues [35]) are conserved and cells can attach, spread and proliferate on the porous hydrogels surface without any washing or post formulation treatments. Of particular interest, cell behaviour and morphology could still be modulated through the conserved ability to tune the DGL/PEG hydrogels mechanical properties by varying their compositions.

In addition to be non-cytotoxic, injected porous matrices should allow cells to swiftly enter and colonize the structure to support in-depth tissue formation [70,71,48]. The important interconnection obtained in EPH allows the cells to rapidly and homogenously infiltrate the entire porous structure thereby creating tissue. Similarly, once injected in mice for 3 weeks, the porous structure formed directly *in vivo* allows for an extensive vascularization and cellular infiltration although having a decreased pore size compared with hydrogels injected in tubes. This decreased pore size was correlated with a structure flattening probably due to a combined effect of the skin weight exerting a pressure on the porous hydrogel and the contraction of the panniculus carnosus. However, the porous architecture could be sufficiently maintained to allow cell infiltration and tissue ingrowth for all the conditions studied.

Moreover, the effervescently porous hydrogel could be injected directly *in vivo* while eliciting a mild inflammatory reaction with the presence of macrophages degrading hydrogel walls as previously shown for DGL/PEG systems [35]. The local blood flow around the injected implants and the hydrogel water content are hypothesized to help the diffusion and solubility of CO_2 gas generated by effervescence in the bloodstream and biological tissues, preventing the formation of a gas cavity.

Overall, these results provide a proof-of-principle that the DGL/PEG effervescent porous hydrogel can be injected *in situ* while enabling the formation of a suitable porosity that enhances cellular infiltration, vascularization and tissue deposition, while eliciting a mild inflammatory reaction. Therefore, these innovative porous and injectable hydrogels with tunable mechanical properties offer many perspectives for *in situ* tissue engineering applications.

5. Conclusion

In conclusion, although numerous attempts have been made to develop porous hydrogels able to provide a variety of mechanical cues required by cells and tissues, many failed to provide *in situ* injectability [13,51,60]. On the contrary, injectable hydrogel designed to embark cells *in situ*, generally result in poor cell migration due to sterically hindered spreading, or lack of oxygen and nutrient transport. The effervescent method described herein provides a basis for the synthesis of macroporous multifunctional and highly tunable hydrogels with direct *in vivo* injectable potential. A simple optimization of the acid-base effervescence was carried out to match the DGL/PEG hydrogel crosslinking reaction and enable to entrap generated CO_2 bubbles inside the hydrogel network. Resultant innovative effervescent porous DGL/PEG hydrogels are easily produced *in vivo*, allowing for an extensive vascularization and cellular infiltration, without harming effect on tissues. In further studies, we will evaluate the potential of effervescent porous hydrogels to provide a suitable environment for the repair of muscle volumetric loss. On a wider perspective, the strategy developed herein could be transposed to other biomaterial system of tailorable setting or crosslinking, to create an extensive and highly interconnected porosity using a non-cytotoxic and cell-friendly process suitable for injection, in versatile applications.

Declaration of Competing Interest

The authors declare that they have no known competing financial interests or personal relationships that could have appeared to influence the work reported in this paper.

Acknowledgements

We thank the Agence nationale de la recherche (grant number ANR-17-CE19-0009) and the Centre national de la recherche scientifique for funding. We thank the PrimaTiss platform (Naïma El Kholti) and Novotec for histological stainings. We are grateful to the Institut de génomique fonctionnel de Lyon (IGFL, Sabine Richard) for access to their vibratome.

Supplementary materials

Supplementary material associated with this article can be found, in the online version, at doi:10.1016/j.actbio.2021.11.036.

References

[1] K. Deligkaris, T.S. Tadele, W. Olthuis, A. van den Berg, Hydrogel-based devices for biomedical applications, Sens. Actuators B Chem. 147 (2010) 765–774, https://doi.org/10.1016/j.snb.2010.03.083.
[2] K.Y. Lee, D.J. Mooney, Hydrogels for tissue engineering, Chem. Rev. 101 (2001) 1869–1879, https://doi.org/10.1021/cr000108x.
[3] A.S. Hoffman, Hydrogels for biomedical applications, Adv. Drug Deliv. Rev. 54 (2002) 3–12, S0169-409X(01)00239-3.
[4] A.P. Mathew, S. Uthaman, K.H. Cho, C.S. Cho, I.K. Park, Injectable hydrogels for delivering biotherapeutic molecules, Int. J. Biol. Macromol. (2017), https://doi.org/10.1016/j.ijbiomac.2017.11.113.
[5] E. Piantanida, G. Alonci, A. Bertucci, L. De Cola, Design of nanocomposite injectable hydrogels for minimally invasive surgery, Acc. Chem. Res. (2019), https://doi.org/10.1021/acs.accounts.9b00114.
[6] K. Saekhor, W. Udomsinprasert, S. Honsawek, W. Tachaboonyakiat, Preparation of an injectable modified chitosan-based hydrogel approaching for bone tissue engineering, Int. J. Biol. Macromol. 15 (2018) 167–173, https://doi.org/10.1016/j.ijbiomac.2018.11.041.
[7] C. Rhim, D.A. Lowell, M.C. Reedy, D.H. Slentz, S.J. Zhang, W.E. Kraus, G.A. Truskey, Morphology and ultrastructure of differentiating three-dimensional mammalian skeletal muscle in a collagen gel, Muscle Nerve 36 (2007) 71–80, https://doi.org/10.1002/mus.20788.
[8] J.P. Beier, J. Stern-Straeter, V.T. Foerster, U. Kneser, G.B. Stark, A.D. Bach, Tissue engineering of injectable muscle: three-dimensional myoblast-fibrin injection in the syngeneic rat animal model, Plast. Reconstr. Surg. 118 (2006) 1113–1121, https://doi.org/10.1097/01.prs.0000221007.97115.1d.
[9] M. Kim, Y. Hwang, G. Tae, The enhanced anti-tissue adhesive effect of injectable pluronic-HA hydrogel by poly(γ-glutamic acid), Int. J. Biol. Macromol. 93 (2016) 1603–1611, https://doi.org/10.1016/j.ijbiomac.2016.02.064.
[10] W. Bensaïd, J.T. Triffitt, C. Blanchat, K. Oudina, L. Sedel, H. Petite, A biodegradable fibrin scaffold for mesenchymal stem cell transplantation, Biomaterials 24 (2003) 2497–2502, https://doi.org/10.1016/S0142-9612(02)00618-X.
[11] G. Jin, S. Lee, S. Kim, M. Kim, J. Jang, Bicomponent electrospinning to fabricate three-dimensional hydrogel-hybrid nanofibrous scaffolds with spatial fiber tortuosity, Biomed. Microdevices 16 (2014) 793–804, https://doi.org/10.1007/s10544-014-9883-z.
[12] V. Kroehne, I. Heschel, F. Schügner, D. Lasrich, J.W. Bartsch, H. Jockusch, Use of a novel collagen matrix with oriented pore structure for muscle cell differentiation in cell culture and in grafts, J. Cell. Mol. Med. 12 (2008) 1640–1648, https://doi.org/10.1111/j.1582-4934.2008.00238.x.
[13] J. Grenier, H. Duval, F. Barou, P. Lv, B. David, D. Letourneur, Mechanisms of pore formation in hydrogel scaffolds textured by freeze-drying, Acta Biomater. (2019), https://doi.org/10.1016/j.actbio.2019.05.070.
[14] Y.C. Chiu, M.H. Cheng, H. Engel, S.W. Kao, J.C. Larson, S. Gupta, E.M. Brey, The role of pore size on vascularization and tissue remodeling in PEG hydrogels, Biomaterials 32 (2011) 6045–6051, https://doi.org/10.1016/j.biomaterials.2011.04.066.
[15] V. Guarino, M. Galizia, M. Alvarez-perez, G. Mensitieri, L. Ambrosio, Improving surface and transport properties of macroporous hydrogels for bone regeneration, J. Biomed. Mater. Res. Part A 103A (2014) 1095–1105, https://doi.org/10.1002/jbm.a.35246.
[16] R.S. Moglia, J.L. Holm, N.A. Sears, C.J. Wilson, D.M. Harrison, E. Cosgriff-Hernandez, Injectable polyHIPEs as high-porosity bone grafts, Biomacromolecules 12 (2011) 3621–3628, https://doi.org/10.1021/bm2008839.
[17] R.S. Moglia, M. Whitely, P. Dhavalikar, J. Robinson, H. Pearce, M. Brooks, M. Stuebben, N. Cordner, E. Cosgriff-Hernandez, Injectable polymerized high internal phase emulsions with rapid *in situ* curing, Biomacromolecules 15 (2014) 2870–2878, https://doi.org/10.1021/bm500754r.
[18] N.R. Cameron, High internal phase emulsion templating as a route to well-defined porous polymers, Polymer 46 (2005) 1439–1449, https://doi.org/10.1016/j.polymer.2004.11.097, Guildf.
[19] N. Annabi, S.M. Mithieux, A.S. Weiss, F. Dehghani, The fabrication of elastin-based hydrogels using high pressure CO_2, Biomaterials 30 (2009) 1–7, https://doi.org/10.1016/j.biomaterials.2008.09.031.
[20] B.S. Partap, I. Rehman, J.R. Jones, J.A. Darr, Supercritical carbon dioxide in water " emulsion-templated synthesis of porous calcium alginate hydrogels **, Adv. Mater. (2006) 501–504, https://doi.org/10.1002/adma.200501423.
[21] C. Palocci, A. Barbetta, A. La Grotta, M. Dentini, R... April, I. Final, F. May, Porous biomaterials obtained using supercritical CO_2-water emulsions, Langmuir 23 (2007) 8243–8251, https://doi.org/10.1021/la700947g.
[22] N. Annabi, S.M. Mithieux, E.A. Boughton, A.J. Ruys, A.S. Weiss, F. Dehghani, Synthesis of highly porous crosslinked elastin hydrogels and their interaction with fibroblasts *in vitro*, Biomaterials 30 (2009) 4550–4557, https://doi.org/10.1016/j.biomaterials.2009.05.014.
[23] N. Annabi, S.M. Mithieux, A.S. Weiss, F. Dehghani, Cross-linked open-pore elastic hydrogels based on tropoelastin, elastin and high pressure CO_2, Biomaterials 31 (2010) 1655–1665, https://doi.org/10.1016/j.biomaterials.2009.11.051.
[24] L. Wang, S. Dong, Y. Liu, Y. Ma, J. Zhang, Z. Yang, W. Jiang, Y. Yuan, Fabrication of injectable, porous hyaluronic acid hydrogel based on an *in-situ* bubble-forming hydrogel entrapment process, Polymers 12 (2020), https://doi.org/10.3390/polym12051138, Basel.
[25] N. Annabi, J.W. Nichol, D. Ph, X. Zhong, C. Ji, Controlling the porosity and microarchitecture of hydrogels for tissue engineering, Tissue Eng. Part B Rev. 16 (2010).
[26] D.J. Mooney, D.F. Baldwin, N.P. Suht, J.P. Vacantis, R. Larger, Novel approach to fabricate porous sponges of poly (D,L-lactic-co-glycolic acid) without the use of organic solvents, Biomaterials 17 (1996) 1417–1422.
[27] F. Dehghani, N. Annabi, P. Valtchev, S.M. Mithieux, A.S. Weiss, S.G. Kazarian, F.H. Tay, Effect of dense gas CO_2 on the coacervation of elastin, Biomacromolecules 9 (2008) 1100–1105.
[28] M.A. Winters, B.L. Knutson, P.G. Debenedetti, H.G. Sparks, T.M. Przybycien, C.L. Stevenson, S.J. Prestrelski, Precipitation of proteins in supercritical carbon dioxide, J. Pharm. Sci. (1996) 85.
[29] S. Hesaraki, F. Moztarzadeh, D. Sharifi, Formation of interconnected macropores in apatitic calcium phosphate bone cement with the use of an effervescent additive, J. Biomed. Mater. Res. 83 (2007) 80–87, https://doi.org/10.1002/jbm.a.
[30] V. Keskar, N. Marion, J.J. MAo, R.A. Gemeinhart, *In vitro* evaluation of macroporous hydrogels to facilitate stem cell infiltration, growth, and mineralization, Tissue Eng. Part A 15 (2009).
[31] W. Tachaboonyakiat, T. Furubayashi, M. Katoh, T. Ooya, N. Yui, Novel biodegradable cholesterol-modified polyrotaxane hydrogels for cartilage regeneration, J. Biomater. Sci. Polym. Ed. 15 (2004) 1389–1404, https://doi.org/10.1163/1568562042368086.
[32] Y.M. Ju, K. Park, J.S. Son, J.J. Kim, J.W. Rhie, D.K. Han, Beneficial effect of hydrophilized porous polymer scaffolds in tissue-engineered cartilage formation, J. Biomed. Mater. Res. Part B Appl. Biomater. 85 (2008) 252–260, https://doi.org/10.1002/jbm.b.30943.
[33] A. Fernández-Colino, F. Wolf, H. Keijdener, S. Rütten, T. Schmitz-Rode, S. Jockenhoevel, J.C. Rodríguez-Cabello, P. Mela, Macroporous click-elastin-like hydrogels for tissue engineering applications, Mater. Sci. Eng. C 88 (2018) 140–147, https://doi.org/10.1016/j.msec.2018.03.013.
[34] K. Kabiri, H. Omidian, M.J. Zohuriaan-Mehr, Novel approach to highly porous superabsorbent hydrogels: synergistic effect of porogens on porosity and swelling rate, Polym. Int. 52 (2003) 1158–1164, https://doi.org/10.1002/pi.1218.
[35] M. Carrancá, L. Griveau, N. Remoué, C. Lorion, P. Weiss, V. Orea, D. Sigaudo-Roussel, C. Faye, D. Ferri-Angulo, R. Debret, J. Sohier, Versatile lysine dendrigrafts and polyethylene glycol hydrogels with inherent biological properties: *in vitro* cell behavior modulation and *in vivo* biocompatibility, J. Biomed. Mater. Res. Part A (2020), https://doi.org/10.1002/jbm.a.37083.
[36] C. Lorion, C. Faye, B. Maret, T. Trimaille, T. Régnier, P. Sommer, R. Debret, Biosynthetic support based on dendritic poly(L-lysine) improves human skin fibroblasts attachment, J. Biomater. Sci. Polym. Ed. 25 (2014) 136–149, https://doi.org/10.1080/09205063.2013.843966.
[37] Z. Chen, B. Chen, X.Q. Yao, B.S. Gui, Y. Ou, J.M. Ouyang, Anticoagulation of diethyl citrate and its comparison with sodium citrate in an animal model, Blood Purif. 33 (2012) 30–36, https://doi.org/10.1159/000330891.
[38] W. Melzer, A. Herrmann-Frank, H.C. Lüttgau, The role of Ca2+ ions in excitation-contraction coupling of skeletal muscle fibres, Biochim. Biophys. Acta 1241 (1995) 59–116, https://doi.org/10.1016/0304-4157(94)00014-5.
[39] I. Levental, P.C. Georges, P.A. Janmey, Soft biological materials and their impact on cell function, Soft Matter 3 (2007) 299–306, https://doi.org/10.1039/b610522j.
[40] A.J. Engler, S. Sen, H.L. Sweeney, D.E. Discher, Matrix elasticity directs stem cell lineage specification, Cell 126 (2006) 677–689, https://doi.org/10.1016/j.cell.2006.06.044.
[41] P. Trivedi, T. Saloranta-Simell, U. Maver, L. Gradišnik, N. Prabhakar, J.H. Smått, T. Mohan, M. Gericke, T. Heinze, P. Fardim, Chitosan–cellulose multifunctional hydrogel beads: Design, characterization and evaluation of cytocompatibility with breast adenocarcinoma and osteoblast cells, Bioengineering 5 (2018), https://doi.org/10.3390/bioengineering5010003.
[42] S. Sarda, M. Nilsson, M. Balcells, E. Fernández, Influence of surfactant molecules as air-entraining agent for bone cement macroporosity, J. Biomed. Mater. Res. (2002) 215–221, https://doi.org/10.4028/www.scientific.net/KEM.218-220.335.

[43] R.A. Gemeinhart, H. Park, K. Park, Pore structure of superporous hydrogels, Polym. Adv. Technol. 11 (2000) 617–625, 10.1002/1099-1581(200008/12)11:8/12<617::AID-PAT12>3.0.CO;2-L.

[44] N. Gupta, H. Shivakumar, Preparation and characterization of superporous hydrogels as pH-sensitive drug delivery system for pantoprazole sodium, DARU J. Pharm. Sci. 18 (2010) 505–510, https://doi.org/10.2174/156720109789941722.

[45] J. Chen, H. Park, K. Park, Synthesis of superporous hydrogels: Hydrogels with fast swelling and superabsorbent properties, J. Biomed. Mater. Res. 44 (1999) 53–62, 10.1002/(SICI)1097-4636(199901)44:1<53::AID-JBM6>3.0.CO;2-W.

[46] J. Jankolovits, Studying pH dependence of a peptide modification with an N-hydroxysuccinimide ester using mass spectrometry, J. Young Investig. 15 (2006), October.

[47] J.P. Francoia, J.C. Rossi, G. Monard, L. Vial, Digitizing poly-L-lysine dendrigrafts: from experimental data to molecular dynamics simulations, J. Chem. Inf. Model. 57 (2017) 2173–2180, https://doi.org/10.1021/acs.jcim.7b00258.

[48] L. Huang, J. Huang, H. Shao, X. Hu, C. Cao, S. Fan, L. Song, Y. Zhang, Silk scaffolds with gradient pore structure and improved cell infiltration performance, Mater. Sci. Eng. C. 94 (2019) 179–189, https://doi.org/10.1016/j.msec.2018.09.034.

[49] S. Sokic, M. Christenson, J. Larson, G. Papavasiliou, *In situ* generation of cell-laden porous MMP-sensitive PEGDA hydrogels by gelatin leaching, Macromol. Biosci. 14 (2014) 731–739, https://doi.org/10.1002/mabi.201300406.

[50] J. Wu, Y. Hong, Enhancing cell infiltration of electrospun fibrous scaffolds in tissue regeneration, Bioact. Mater. 1 (2016) 56–64, https://doi.org/10.1016/j.bioactmat.2016.07.001.

[51] L. Martín, M. Alonso, A. Girotti, F.J. Arias, J.C. Rodríguez-Cabello, Synthesis and characterization of macroporous thermosensitive hydrogels from recombinant elastin-like polymers, Biomacromolecules 10 (2009) 3015–3022, https://doi.org/10.1021/bm900560a.

[52] I. Bružauskaitė, D. Bironaitė, E. Bagdonas, E. Bernotienė, Scaffolds and cells for tissue regeneration: different scaffold pore sizes-different cell effects, Cytotechnology 68 (2016) 355–369, https://doi.org/10.1007/s10616-015-9895-4.

[53] N. Abbasi, S. Hamlet, R.M. Love, N.T. Nguyen, Porous scaffolds for bone regeneration, J. Sci. Adv. Mater. Devices 5 (2020) 1–9, https://doi.org/10.1016/j.jsamd.2020.01.007.

[54] S.. Hulbert, F.A. Young, R.S. Mathews, J.. Klawitter, C.D. Talbert, F. Stelling, Potential of ceramic materials as permanently implantable skeletal prosthesis, 4 (1970) 433–456.

[55] S. Jana, A. Cooper, M. Zhang, Chitosan scaffolds with unidirectional microtubular pores for large skeletal myotube generation, Adv. Healthc. Mater. 2 (2013) 557–561, https://doi.org/10.1002/adhm.201200177.

[56] J.P. Beier, D. Klumpp, M. Rudisile, R. Dersch, J.H. Wendorff, O. Bleiziffer, A. Arkudas, E. Polykandriotis, R.E. Horch, U. Kneser, Collagen matrices from sponge to nano : new perspectives for tissue engineering of skeletal muscle, BMC Biotechnol. 14 (2009) 1–14, https://doi.org/10.1186/1472-6750-9-34.

[57] C.M. Murphy, G.P. Duffy, A. Schindeler, J.O. Fergal, Effect of collagen-glycosaminoglycan scaffold pore size on matrix mineralization and cellular behavior in different cell types, J. Biomed. Res. Part A 104A (2016) 291–304, https://doi.org/10.1002/jbm.a.35567.

[58] E. Tsuruga, H. Takita, H. Itoh, Y. Wakisaka, Y. Kuboki, Pore size of porous hydroxyapatite as the controls BMP-induced osteogenesis, J. Biochem. 121 (1997) 317–324.

[59] L. Zeng, Y. Yao, D. Wang, X. Chen, Effect of microcavitary alginate hydrogel with different pore sizes on chondrocyte culture for cartilage tissue engineering, Mater. Sci. Eng. C 34 (2014) 168–175, https://doi.org/10.1016/j.msec.2013.09.003.

[60] B. Jiang, T.M. Waller, J.C. Larson, A.A. Appel, E.M. Brey, Fibrin-Loaded porous poly(ethylene glycol) hydrogels as scaffold materials for vascularized tissue formation, Tissue Eng. Part A 19 (2013) 224–234, https://doi.org/10.1089/ten.tea.2012.0120.

[61] O. Yom-Tov, L. Neufeld, D. Seliktar, H. Bianco-Peled, A novel design of injectable porous hydrogels with *in situ* pore formation, Acta Biomater. 10 (2014) 4236–4246, https://doi.org/10.1016/j.actbio.2014.07.006.

[62] X. Xiao, W. Wang, D. Liu, H. Zhang, P. Gao, L. Geng, Y. Yuan, J. Lu, Z. Wang, The promotion of angiogenesis induced by three-dimensional porous beta-tricalcium phosphate scaffold with different interconnection sizes via activation of PI3K/Akt pathways, Sci. Rep. 5 (2015) 1–11, https://doi.org/10.1038/srep09409.

[63] M. Mastrogiacomo, S. Scaglione, R. Martinetti, L. Dolcini, F. Beltrame, R. Cancedda, R. Quarto, Role of scaffold internal structure on *in vivo* bone formation in macroporous calcium phosphate bioceramics, Biomaterials 27 (2006) 3230–3237, https://doi.org/10.1016/j.biomaterials.2006.01.031.

[64] F. Bai, Z. Wang, J. Lu, J. Liu, G. Chen, R. Lv, J. Wang, K. Lin, J. Zhang, X. Huang, The correlation between the internal structure and vascularization of controllable porous bioceramic materials *in vivo*: a quantitative study, Tissue Eng. Part A 16 (2010) 3791–3803, https://doi.org/10.1089/ten.tea.2010.0148.

[65] S.I. Somo, B. Akar, E.S. Bayrak, J.C. Larson, A.A. Appel, H. Mehdizadeh, A. Cinar, E.M. Brey, Pore interconnectivity influences growth factor-mediated vascularization in sphere-templated hydrogels, Tissue Eng. Part C Methods 21 (2015) 773–785, https://doi.org/10.1089/ten.tec.2014.0454.

[66] J.E. Babensee, J.M. Anderson, L.V. McIntire, A.G. Mikos, Host response to tissue engineered devices, Adv. Drug Deliv. Rev. 33 (1998) 111–139, https://doi.org/10.1016/S0169-409X(98)00023-4.

[67] R. Klopfleisch, F. Jung, The pathology of the foreign body reaction against biomaterials, J. Biomed. Res. Part A 105A (2017) 927–940, https://doi.org/10.1002/jbm.a.35958.

[68] S. Ullm, A. Krüger, C. Tondera, T.P. Gebauer, A.T. Neffe, A. Lendlein, F. Jung, J. Pietzsch, Biocompatibility and inflammatory response *in vitro* and *in vivo* to gelatin-based biomaterials with tailorable elastic properties, Biomaterials 35 (2014) 9755–9766, https://doi.org/10.1016/j.biomaterials.2014.08.023.

[69] P.J. VandeVord, H.W.T. Matthew, S.P. DeSilva, L. Mayton, B. Wu, P.H. Wooley, Evaluation of the biocompatibility of a chitosan scaffold in mice, J. Biomed. Mater. Res. 59 (2002) 585–590, https://doi.org/10.1002/jbm.1270.

[70] B.J. Lawrence, S.V. Madihally, Cell colonization in degradable 3D porous matrices, Cell Adh. Migr. 2 (2008) 9–16.

[71] C.J. Rivet, K. Zhou, R.J. Gilbert, D.I. Finkelstein, J.S. Forsythe, Cell infiltration into a 3D electrospun fiber and hydrogel hybrid scaffold implanted in the brain, Biomatter 5 (2015).